A Catchment-Based Hydrologic and Routing Modeling System with explicit river channels

Gopi Goteti,[1] James S. Famiglietti,[1] and Kwabena Asante[2]

Received 8 December 2007; revised 24 March 2008; accepted 29 April 2008; published 22 July 2008.

[1] In this paper, we present a macroscale hydrologic modeling system with an explicit representation of storage and movement of water in river channels and floodplains. The overall modeling system, called the Catchment-Based Hydrologic and Routing Modeling System (CHARMS), is composed of a land surface model and a river routing model that operate on a network of hydrologic catchments (or watersheds). The land surface model in CHARMS is based on the National Center for Atmospheric Research Community Land Model. The river routing model in CHARMS generates river discharge by transporting runoff generated by the catchment-based CLM through the river network. The routing model uses information on channel cross-section geometry, derived from the 90 m Shuttle Radar Topography Mission digital elevation model, to simulate river discharge and the associated flow depth and inundation width. CHARMS was implemented over the Wabash River basin in the central United States (drainage area 72282 km^2), and simulated streamflow was validated using daily observations. Simulated flow depth and inundation extent generally followed seasonal variations in observed flooding and droughts. Limitations of some of the assumptions and scaling factors used in this study and the issues that need to be addressed for a continental- or global-scale implementation of CHARMS are discussed. This paper serves as the foundation for a catchment-based, global land surface modeling framework that could incorporate spatiotemporal variations in surface water bodies, as well as satellite measurements of these variations.

Citation: Goteti, G., J. S. Famiglietti, and K. Asante (2008), A Catchment-Based Hydrologic and Routing Modeling System with explicit river channels, *J. Geophys. Res.*, *113*, D14116, doi:10.1029/2007JD009691.

1. Introduction

[2] The terrestrial hydrologic cycle is inseparably connected with the energy and biogeochemical cycles and plays an important role in land-atmosphere and land-ocean interactions. Hence, knowledge of terrestrial water storage and movement is important not only for water resources management, but for understanding land-atmosphere exchange of CO_2 [e.g., *Richey et al.*, 2002], the role of surface water bodies in regulating regional climate [e.g., *Coe and Bonan*, 1997], sediment [e.g., *Syvitski et al.*, 2005] and nutrient fluxes [e.g., *Green et al.*, 2004] to the coastal ocean and changes in ocean circulation due to continental freshwater inputs [e.g., *Rahmstorf*, 1996]. A unique opportunity to understand variations in surface water movement and storage and the cycling of water through the Earth system is presented by increasingly available satellite observations of river and lake elevations [e.g., *Birkett et al.*, 2002], data on global inundation extent [*Prigent et al.*, 2007] and fine resolution topographic data [*Lehner et al.*, 2006]. However, land surface models (LSMs), which are the only available tools to simulate the terrestrial hydrologic cycle at continental and global scales, lack an adequate representation of spatiotemporal variations in surface water storage and movement. The primary objective of this work is to improve river transport and floodplain water storage components for use in LSMs.

[3] Within each LSM modeling unit (i.e., a latitude-longitude grid box), LSMs estimate surface and subsurface runoff, along with other hydrological fluxes, taking into account the meteorological conditions, land cover and soil characteristics and antecedent soil moisture conditions. A river routing model then transports the simulated runoff from the continental interiors, through the river channels, to lakes and/or oceans. In runoff production calculations, many LSMs account for heterogeneity in land cover and topography within a model grid (i.e., subgrid heterogeneity). In contrast, routing models employed by these LSMs [e.g., *Miller et al.*, 1994] and other continental-scale routing models [e.g., *Fekete et al.*, 2002] assume each grid to be homogenous. At the typical LSM resolutions of $\frac{1}{2}^0$ ($\sim$2500 km^2) or 1^0 ($\sim$10000 km^2), spatiotemporal variations in rivers, floodplains, lakes, wetlands and other surface water bodies can never be modeled realistically, because

[1]Department of Earth System Science, University of California, Irvine, California, USA.
[2]Geospatial Science and Engineering, South Dakota State University, Brookings, South Dakota, USA.

0148-0227/08/2007JD009691

these variations are controlled by features much finer than the resolution of the LSM.

[4] Some studies have attempted to address this drawback of routing models using conceptualized representations of subgrid features [e.g., *Vorosmarty et al.*, 1989; *Coe et al.*, 2002; *Doll et al.*, 2003; *Miguez-Macho et al.*, 2007], by using precipitation and streamflow data to deduce a response function that represents the subgrid control on runoff transport [e.g., *Lohmann et al.*, 1996], or by interpolating coarse resolution LSM runoff to a finer-scale grid on which routing is performed [e.g., *Yu et al.*, 2006]. Although such models are useful in water resources assessment studies, improved representation of subgrid features is not always feasible within the latitude-longitude computational grid structure used by these and other existing models. For instance, a realistic incorporation of river channels and floodplains (and other water bodies) would require LSMs to be implemented at a very fine resolution (e.g., 1 km), which is not computationally feasible in a global implementation within climate models. Similarly, using a spatially explicit floodplain hydraulic model such as the LISFLOOD model of *Bates and DeRoo* [2000] within an LSM would require enormous computational resources. In addressing the drawbacks of existing grid-based routing models, catchment-based models provide a unique and viable solution.

1.1. Catchment-Based Models

[5] The modeling unit in a catchment-based model is the natural catchment, as opposed to the latitude-longitude (lat-lon) grid used in most LSMs. Note that the term catchment is used in this paper in the context of a drainage area that is similar in size to a lat-lon grid box, and the term drainage basin in the context of a larger drainage region (e.g., Colorado River basin). Catchment boundaries coincide with natural topographic divides, and the stream network defines river flow paths. In a catchment-based model, the movement of river discharge takes place through channels that follow the actual path of the river. Hence, channel cross-sectional geometry could be used to estimate channel and floodplain storage at any point on the river network. Since surface water storage and movement are also controlled by topography, incorporation of subcatchment heterogeneity in the transport and storage of runoff is much more feasible in a catchment-based model compared to its grid-based counterpart. Thus, using computational resources similar to that of grid-based models, catchment-based models have the potential to realistically simulate the movement and storage of runoff and the associated spatiotemporal variations in surface water storage.

[6] Some studies have used the hydrologic catchment as the fundamental modeling unit. For instance, *Koster et al.* [2000] and its follow-on studies [e.g., *Reichle and Koster*, 2005] estimate land-atmosphere fluxes at continental and global scales on a catchment-based modeling template. However, *Koster et al.* [2000] and other existing catchment-based models [e.g., *Kite et al.*, 1994; *Chen and Kumar*, 2001] do not incorporate surface water bodies and have not attempted to simulate spatial and temporal changes in surface water storage resulting from transport of runoff.

1.2. Objectives

[7] This study presents a catchment-based routing model, which operates within a catchment-based LSM framework, with an explicit representation of river channels and floodplains. This study is an important step toward fully utilizing actual information on channel cross-section geometry and explicitly simulating depths and inundation extents associated with discharge in river channels, all within the framework of a LSM. This work is also a first step toward the long-term objective of building a global catchment-based land surface modeling framework capable of simulating spatial and temporal variations in surface water bodies consistent with coupled Earth System models. Such a framework will ultimately enable assimilation of satellite observations of surface water heights and inundation extents [e.g., *Andreadis et al.*, 2007], the incorporation of water management practices (such as reservoir storage [e.g., *Hanasaki et al.*, 2006]), linkages to biogeochemical processes and related feedbacks to climate.

1.3. Overall Approach

[8] The grid-based National Center for Atmospheric Research (NCAR) Community Land Model (CLM) was modified to run on a catchment-based modeling template. The catchment-based CLM was coupled to a catchment-based river routing model, described in this paper, which simulates the movement of water through river channels and floodplains. The overall framework, called the Catchment-Based Hydrologic and Routing Modeling System (henceforth referred to as CHARMS) was implemented over the Wabash River basin and simulated daily streamflow was validated using observations. Along with channel cross-section profile information, CHARMS was used to estimate depth and floodplain inundation extent associated with the simulated discharge. The remainder of this paper is organized as follows. The data sets used in this study are described in section 2. The models used in this work are described in section 3. Results from the model implementation are presented in section 4. Future research work is outlined in section 5 and an overall summary is provided in section 6.

2. Data

[9] The catchment-based routing model in CHARMS does not yet account for flow regulation (dams, reservoirs, etc.) or lake water storage. Consequently, the choice of the study region was dependent upon the availability of unregulated streamflow data, the absence of any major lakes, dams or reservoirs, and the availability of meteorological data. On the basis of the above criteria, the Wabash River basin in central United States (see Figure 1) was chosen as the study region. The data sets described below were chosen because they are suitable, in general, for future implementations of CHARMS at continental or global scale and also for coupled land-atmosphere simulations.

2.1. Topographic Data

[10] Elevation data are required for the delineation of catchment boundaries and river flow paths in CHARMS. In this study, we use the 30 arc sec ($\sim$1 km) digital elevation model (DEM) data from GTOPO30 (from http://eros.usgs.

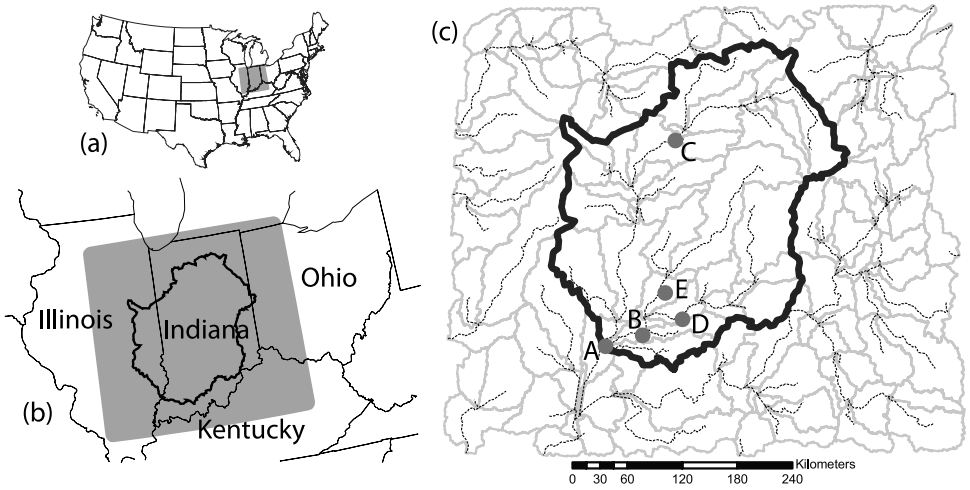

Figure 1. (a) The region of study (shaded portion) with reference to conterminous USA. (b) An enlarged view of the study region, with the thick solid line showing the extent of the Wabash River basin upstream of USGS gage 03377500 at Mt. Carmel, IL (station A in Figure 1c, at right). (c) Network of catchments and river channels obtained using ArcHydro. Rivers are indicated by dotted lines, and catchment boundaries are indicated by grey lines. Thick solid line indicates the simulated extent of the Wabash River basin (72282 km^2). The mean size of a catchment in the Wabash basin is 1902 km^2 with a standard deviation of 1694 km^2. The grey circles (A through E) are the five HCDN/USGS streamflow gaging stations used in this study (see Table 1).

gov/products/elevation.html). Raw DEM data from GTOPO30 was processed by *Asante* [2000], and corrected for spurious depressions in the terrain, to create global DEM data suitable for continental-scale modeling studies. Topographic indices required by the CLM runoff scheme [*Niu et al.*, 2005] (see section 3.2) for the computation of maximum fractional saturated area were obtained from HYDRO1k (available from http://edc.usgs.gov/products/elevation/gtopo30/hydro/index.html). River channel cross-section profiles required by the routing model in CHARMS were derived from the 3 arc sec (~90 m) Shuttle Radar Topography Mission (SRTM [*Farr et al.*, 2007]) DEM.

2.2. Land Cover Data

[11] Soil properties, soil depths and vegetation cover characteristics were based on the input data used by the current version of the grid-based CLM [see *Bonan et al.*, 2002].

2.3. Meteorological Data

[12] The CLM is forced with a suite of atmospheric meteorological data that is typical of LSMs. Forcing variables include, precipitation, air temperature, downward shortwave and longwave radiation, surface pressure, specific humidity and wind speed. Precipitation data was from the observation-based gridded data set of *Maurer et al.* [2002] (1949–2000, daily, $\frac{1}{8}^0$). The remainder of the forcing variables were from the bias-corrected reanalysis data set of *Sheffield et al.* [2006] (1948–2000, 3-hourly, 1^0).

2.4. Streamflow Data

[13] This study uses streamflow data from the Hydro-Climatic Data Network (HCDN [*Slack and Landwehr*, 1992]), a database of U.S. Geological Survey (USGS) streamflow measurements (roughly spanning the period 1874–1988) that have been identified to be relatively free of anthropogenic influences. Daily streamflow data from five HCDN/USGS stations (see Table 1) were used in this study.

3. CHARMS

[14] The two unique features of CHARMS are (1) both the LSM and the routing model operate on a catchment template and (2) both the LSM and the routing model parameterize subcatchment scale variation in topography. Moreover, the routing algorithm in CHARMS includes an explicit representation of river channels and floodplains, and uses channel cross-section information to estimate depth and inundation extent associated with river discharge. These features of CHARMS are important for simulating surface and subsurface storage and transport of water.

3.1. Modeling Template

[15] The ArcHydro terrain processing model [*Maidment*, 2002], a Geographic Information System (GIS)-based computer program, was used to delineate catchment boundaries and river flow paths. ArcHydro is similar to existing terrain analysis algorithms [e.g., *Jenson and Domingue*, 1988], and uses fine resolution DEM data to identify river flow directions, river flow paths and catchment boundaries. The corrected 30 arc sec DEM from *Asante* [2000] (see section 2.1) was used in ArcHydro to derive a network of rivers and catchments (see Figure 1) that forms the modeling template for CHARMS.

3.2. Catchment-Based Land Surface Model

[16] The land surface model used in this study is derived from the grid-based CLM (CLM3.0). This version of the CLM code was modified to incorporate some of the latest changes to CLM (CLM3.5, see http://www.cgd.ucar.edu/tss/clm/), most noteworthy of which is the TOPMODEL-based

Table 1. Five HCDN Streamflow Gaging Stations (A, B, C, D, and E) Shown in Figure 1[a]

Station ID	Station Name	Drainage Area	
		HCDN	ArcHydro [CHARMS]
03377500 (A)	Wabash River, Mt. Carmel, IL	74165	−2.5% [−2.5%]
03374000 (B)	White River, Petersburg, IN	28814	−4.1% [−4.2%]
03335500 (C)	Wabash River, Lafayette, IN	18822	−3.5% [−4.0%]
03373500 (D)	East Fork White River, Shoals, IN	12761	−1.0% [−3.8%]
03360500 (E)	White River, Newberry, IN	12142	−5.7% [−4.3%]

[a]Station ID refers to the HCDN/USGS identification number. Simulated drainage area from ArcHydro is expressed as percentage deviation from the HCDN value (in km^2). The values given within square braces correspond to the drainage area represented in CHARMS.

runoff formulation [*Niu et al.*, 2005] that uses statistics of topography to account for the subgrid heterogeneity in soil moisture distribution after *Famiglietti and Wood* [1994]. The grid-based CLM model code was modified to operate on the catchment modeling template developed in section 3.1. The resulting catchment-based CLM requires that the grid-based forcing and input data described in section 2 be interpolated to the catchment template. The redistribution of grid-based CLM data to the catchment template was performed in a GIS during model setup. Each catchment-based input variable (land cover and meteorological data) was computed as an area-weighted sum of the corresponding variable from all the grid cells in which the catchment resides. The GIS program computes the weights for the above interpolation procedure as the proportion of the catchment area in each of the grid cells. This procedure ensures that subgrid variations of input variables, such as land cover attributes, are generally preserved in the resulting catchment modeling units. Moreover, the difference between simulated runoff, aggregated over the whole study region, from the grid-based CLM and the catchment-based CLM was found to be minimal.

[17] Given these forcings and input variables, the catchment-based CLM performs the same water and energy balance computations as the grid-based CLM, to generate a time series of surface and subsurface (base flow) runoff for each catchment shown in Figure 1. Surface and subsurface runoff from the catchment-based CLM are fed to the routing model, which then simulates river and floodplain discharge, and the associated flow depth and inundation extent.

3.3. Catchment-Based Routing Model

[18] The routing model presented here simulates streamflow in river channels and floodplains and the associated depth and extent of flow. The routing model in CHARMS is implemented in an offline mode with no dynamic interaction with the LSM at this point in time. In each modeling unit of CHARMS (see Figure 2), the river channel is divided into reaches of length L_c [L] with a contributing drainage area of A_h [L^2]. The routing model estimates discharge at the upstream and downstream sections of each of those reaches, accounting for the flow contribution from the hillslopes as well as from any upstream reaches. The parameters L_c (minimum value of 15 km, wherever possible) and A_h associated with each reach are determined from the 30 arc sec DEM using a GIS. Within each routing reach, all surface and subsurface runoff is assumed to traverse an average distance of L_h [L] on the hillslopes before joining the river channel flow. For ease of computation, L_h in this study is defined as $L_h = 0.5 * L_c$. Offline simulations, not shown here, indicate that the above formulation of L_h generally has a minimal effect on the daily streamflow. In the future, L_h for each routing reach will be defined as the average distance from a 1-km pixel to the end of the routing reach and will be computed using digital terrain analysis. The flow paths L_c and L_h are represented as straight lines within the routing model.

3.3.1. Transport From Hillslopes to the River Channel

[19] The catchment-based CLM provides surface and subsurface runoff as depth of water per unit time (units of LT^{-1}). Given that the typical length of a routing reach within a catchment is 20 km and considering the differences between the rate of surface and subsurface flows, transport of runoff from the hillslopes needs to be accounted for a better simulation of daily streamflow. The formulation of the average travel time is from *Lee and Chang* [2005] who used a kinematic-wave approximation and Darcy's law to estimate travel times for surface ($T_{h,surf}$) and subsurface ($T_{h,base}$) runoff, respectively.

$$T_{h,surf} = \left(\frac{n_o \, L_h \, \sqrt{S_h}}{r_{surf}^{2/3}(\tau)} \right)^{3/5} \Big/ \Delta T \tag{1}$$

$$T_{h,base} = \left(\frac{\phi \, L_h}{\kappa \, S_h} \right) \Big/ \Delta T \tag{2}$$

The travel times are expressed in dimensionless form in (1) and (2), where ΔT [T] is the temporal resolution of the routing model, and τ [T] (= ΔT) is a generic routing model time interval. In (1) and (2), n_o is the overland surface roughness coefficient (assumed to be 0.5 throughout this study), S_h is the dimensionless average slope of the hillslope, and $r_{surf}(\tau)$ [LT^{-1}] is surface runoff generated within τ, ϕ is soil porosity and κ is hydraulic conductivity. In this study, S_h was assumed to be a constant value of 0.02% for all the catchments. In future implementations of CHARMS, S_h will be determined from analysis of digital terrain data, as the representative average slope of the hillslope in each routing reach. The fraction of surface or subsurface runoff generated during τ that contributes to the river flow, within the same τ, is given by the response functions associated with surface runoff ($U_{h,surf}$) and subsurface runoff ($U_{h,base}$).

$$U_{h,surf}(\tau) = \frac{1}{T_{h,surf}} \quad \tau = 1, \ldots, T_{h,surf} \tag{3}$$

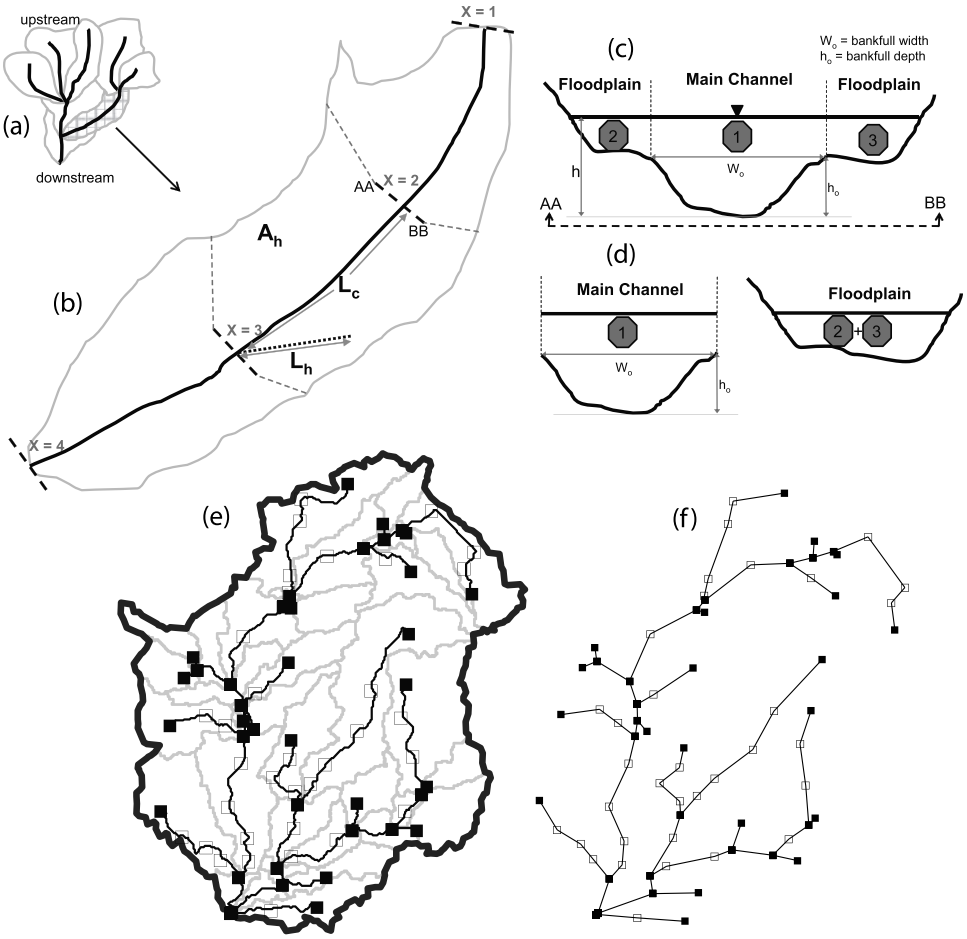

Figure 2. (a) Schematic of a river network (solid black lines) and associated catchment areas (light grey lines). (b) Enlarged view of the shaded catchment. Channel cross sections (X = 1, X = 2, etc.) are indicated by broken black lines, and broken grey lines indicate contributing drainage area (A_h) corresponding to each routing reach. (c) Routing model representation of a channel cross section (e.g., AA-BB in Figure 2b). (d) Total discharge with flow depth h separated into within-channel and floodplain components by the routing model. (e) River channels and associated routing reaches within the Wabash River basin. Shaded squares indicate the beginning and ending of a river channel, and routing reaches are separated by open squares. (f) Routing model representation of the river network.

$$U_{h,base}(\tau) = \frac{1}{T_{h,base}} \quad \tau = 1, \ldots, T_{h,base} \tag{4}$$

The streamflow contribution due to surface runoff ($Q_{h,surf}$) and subsurface runoff ($Q_{h,base}$) within τ is given by,

$$Q_{h,surf}(t) = A_h \sum_{\tau=0}^{\tau=\Lambda} r_{surf}(t-\tau) U_{h,surf}(t-\tau) \tag{5}$$

$$Q_{h,base}(t) = A_h \sum_{\tau=0}^{\tau=\Lambda} r_{base}(t-\tau) U_{h,base}(t-\tau) \tag{6}$$

Here, $r_{base}(\tau)$ $[LT^{-1}]$ is subsurface runoff generated within τ. In order to account for time delays in runoff transport, the above two equations are computed over a period Λ = 30 days. Formulation of runoff transport from the hillslopes using (5) and (6) was done for a physically based simulation of the magnitude and timing of daily total streamflow and its floodplain and main channel components. All the runoff generated by the catchment-CLM does not instantaneously reach the river channel and the travel time, as shown in (1) and (2), is a function of soil characteristics and topography. Unlike the grid-CLM where the routing model has to store runoff information only from the previous time step, the routing model in CHARMS has to store information for several time periods, represented by Λ. By prescribing a value of Λ which is at least as much as the longest travel time of any catchment in the study area, a sufficiently large array is created to store runoff which is still making its way to the river.

3.3.2. Transport Within River Channels and Floodplains

[20] Several previous studies have addressed water transport in river channels. The reader is referred to *Fread* [1993], and the references therein, for a thorough review. The formulation of river transport used here is based on the

studies of *Keefer and McQuivey* [1974], *Becker and Kundzewicz* [1987], *Garbrecht and Brunner* [1991] and *Olivera et al.* [2000]. The structure of the routing model code largely follows that of the Geospatial Streamflow Model (GeoSFM [*Asante et al.*, 2007]).

[21] Consider a control volume spanning the upstream and downstream region of a channel cross section (e.g., AA-BB in Figure 2). At time t [T], h [L] is the depth of flow, W [L] is the width of the flow, Q_{chnl} [L^3T^{-1}] is the flow across the section, A_c [L^2] is the cross-sectional area of flow, and S_{chnl} is the dimensionless slope of the channel bed. Making suitable assumptions, the mass and momentum conservation equations for the control volume can be used to derive the convection-diffusion equation [e.g., see *Cunge et al.*, 1980]. Here, V_c [LT^{-1}] is the convective velocity and D_c [L^2T^{-1}] is the diffusion coefficient. The computation of V_c was accomplished by expressing Q_{chnl} as a power law function of h (see section 3.3.4) and then computing the derivative shown in (8).

$$\frac{\partial Q_{chnl}}{\partial t} + V_c \frac{\partial Q_{chnl}}{\partial x} - D_c \frac{\partial^2 Q_{chnl}}{\partial x^2} = 0 \tag{7}$$

$$V_c = \frac{dQ_{chnl}}{dA_c} = \frac{1}{W} \frac{dQ_{chnl}}{dh} \tag{8}$$

$$D_c = \frac{Q_{chnl}}{2\ W\ S_{chnl}} \tag{9}$$

[22] In order to minimize computational intensity, an analytical rather than a numerical solution of (7) is desirable. For a unit impulse input, the approximate solution of (7) is given by $U_{chnl}(\tau)$ in (10) [*Olivera and Maidment*, 1999]. Thus, $U_{chnl}(\tau)$ can be interpreted as the fraction of the upstream flow that appears at the downstream during the period τ.

$$U_{chnl}(\tau) = \frac{1}{2\tau\sqrt{\pi(\tau/T_c)/\Pi_c}} \exp\left\{ -\frac{[1-(\tau/T_c)]^2}{4(\tau/T_c)/\Pi_c} \right\} \tag{10}$$

Here, the dimensionless quantities T_c and Π_c represent the effect of convective and diffusive processes, respectively, on the propagation of flow.

$$T_c = \left(\frac{L_c}{V_c}\right) \Big/ \Delta T \tag{11}$$

$$\Pi_c = \frac{L_c\ V_c}{D_c} \tag{12}$$

The response function U_{chnl} is computed over a dimensionless time interval ω, given by four standard deviations of U_{chnl} [*Asante*, 2000]: $\omega = 4 * (\sqrt{2\ D_c L_c / V_c^3})/\Delta T$. Thus, U_{chnl} is computed using (10) over the interval ($T_c - \omega/2$, $T_c + \omega/2$) and the values are normalized so that $\sum_{T_c-\omega/2}^{T_c+\omega/2} U_{chnl}(\tau) = 1$. To account for streamflow contributions from previous routing intervals, Q_{chnl} is computed over the period Λ.

$$Q_{chnl}(t, downstream) = \sum_{\tau=0}^{\tau=\Lambda} Q_{chnl}(t-\tau, upstream) U_{chnl}(t-\tau) \tag{13}$$

3.3.3. Extraction of Channel Cross-Section Profiles

[23] Shape of the channel cross section is used by CHARMS to identify main channel and floodplain portions of river channels and to estimate flow depth and inundation extent associated with discharge. River channels were delineated from the raw SRTM DEM. At 1 km increments along the river channel, profiles of sections across (perpendicular to) the river channel were considered. The distance between the centers of adjacent cells in the SRTM DEM is 90 m and 127 m along ordinal and diagonal directions, respectively. Since most rivers do not flow in exactly north–south or east–west directions, a minimum sampling distance of 127 m must be specified. Moreover, the 90th percentile of relative vertical accuracy in SRTM elevation data is between 4 to 10 m globally [*Farr et al.*, 2007]. Hence, the SRTM DEM was sampled at 200 m intervals along each cross section, approximately twice the SRTM DEM resolution, in order to reduce the relative error between adjacent samples by a factor of 2.0.

[24] From each cross-section profile, the width of the channel (W) and the associated cross-sectional area (A_c) and wetted perimeter (P_{wet}) were computed as function of depth (h). Cross-section profiles were extracted only for those river channels of the Wabash River basin that are downstream of the five HCDN stations (see Figure 3a).

[25] In order to assess the adequacy of the SRTM-derived cross sections, field measurements of flow depth (h) and flow width (W) (available from USGS, http://waterdata.usgs.gov/nwis/sw) were compared with corresponding values obtained from SRTM, at three of the five HCDN stations (A, B, and C in Figure 3a) where the observed width of the channel was much larger than the SRTM resolution of 90 m. Furthermore, SRTM-derived h and W data were used in an empirical estimation of discharge (Q), and compared with Q from USGS (corresponding to the field measurements of h and W). The empirical Manning's equation [*Chow*, 1959] was employed to estimate Q from SRTM cross-section profiles.

$$Q = \frac{1}{n}\ A_c\ R^{2/3}\ S_f^{1/2} \tag{14}$$

Here, n is the Manning's roughness coefficient; R is the hydraulic radius, given by $R = A_c/P_{wet}$; and S_f is the friction slope (assumed equal to the slope of the channel bed S_{chnl}).

[26] Comparison of SRTM-derived and observed values of h and W revealed that for a given value of h, W from SRTM is about twice the W from USGS at stations A, B and C. This systematic bias in SRTM W is attributed to the relatively flat terrain in the study area and limitations of the 90 m SRTM DEM in resolving higher-resolution terrain features. Hence, W corresponding to each SRTM h was scaled by a factor of 2.0, resulting in a better comparison of W from SRTM and USGS (see Figure 3b). The SRTM

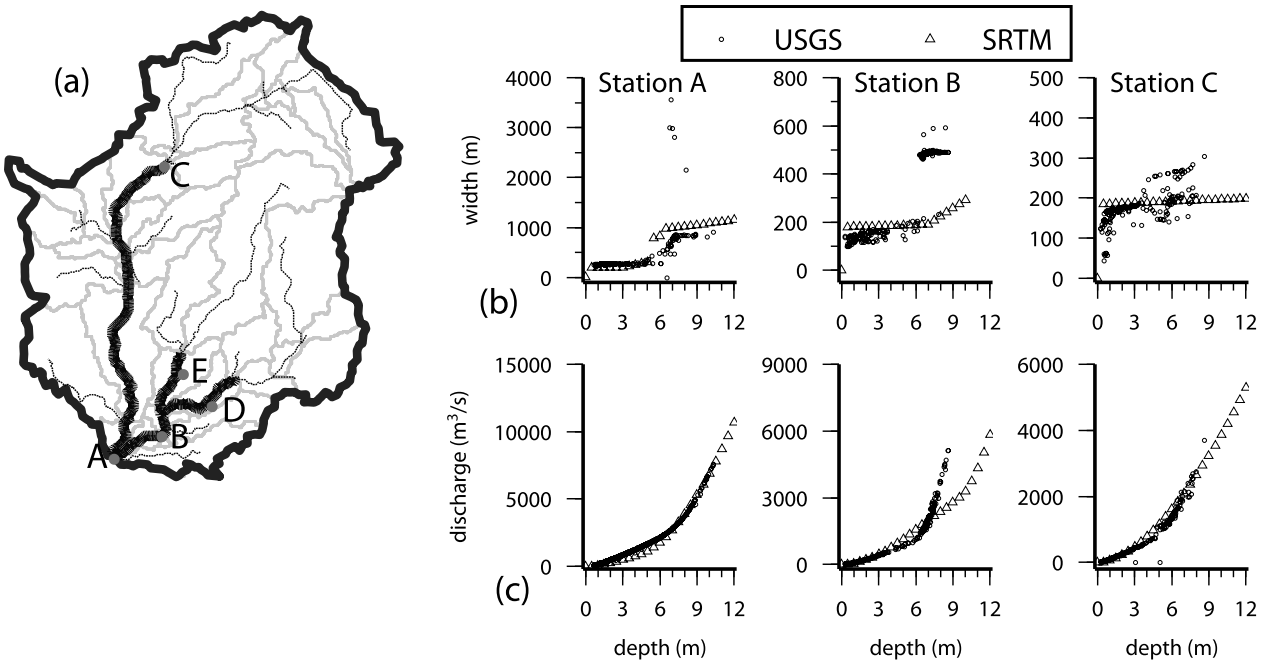

Figure 3. (a) Location of the extracted SRTM cross-section profiles (short solid lines) within the Wabash River basin. The grey circles indicate the locations of the five HCDN stations used in this study. (b) Comparison of flow width versus flow depth measurements from USGS (small open circles) and those extracted from SRTM data (triangles) at stations A, B, and C. Note that the SRTM widths displayed here have been scaled by a factor of 2.0. (c) Discharge corresponding to the USGS measurements of width and depth compared with discharge empirically estimated from SRTM data.

values of h and (scaled) W were then used in (14), separately for the main channel and floodplain, to estimate Q (with S_{chnl} = 0.02%, and n = 0.030 and 0.060, for the main channel and floodplain portions, respectively). The resulting SRTM Q compares reasonably with observed Q from USGS (see Figure 3c). The above comparisons show that SRTM-derived cross-section profiles could be of use in an empirical estimation of flow depth and inundation extent associated with discharge, and vice versa.

[27] To reduce the computational load of the routing model and to compensate for any inconsistencies among the profiles, all cross-section profiles within a routing reach were averaged to obtain an effective cross-section profile for that reach. Furthermore, each effective profile was adjusted for the above mentioned bias in width. Thus, within a catchment, flow depth and inundation extent can vary from one routing reach to another but do not vary within a reach. For catchments with poorly defined SRTM cross-section profiles, channels were assumed to have a constant width of 100 m with no provision for overbank flow (i.e., no floodplain inundation).

3.3.4. Combining Hillslope, Channel, and Floodplain Flows

[28] At each routing model time interval, discharge generated from the hillslopes of every routing reach is computed using (5) and (6). This discharge from the hillslopes directly joins the downstream end of the reach and becomes a part of the inflow to the immediate downstream reach at the next time interval. The total inflow into a reach is the sum of its hillslope discharge and river discharge from any upstream reach. Using the empirical relationship established in section 3.3.3, flow depth and flow width associated with this inflow are estimated. For each effective cross-section profile, bankfull depth (h_o) and bankfull width (W_o) were identified from a visual inspection of the profile. The cross-sectional area of flow is partitioned into within-channel and floodplain portions (see Figure 2) following the power law method of *Garbrecht* [1990]. Then, (8)–(13) are used separately for within-channel and floodplain flows to estimate the resulting downstream flows. Within a reach, there is no mass or momentum exchange between the main channel and the floodplain. The total discharge Q [L^3T^{-1}] at the downstream end of a reach is computed as the sum of the discharge due to surface runoff ($Q_{h,surf}$) and subsurface runoff ($Q_{h,base}$), and the discharge resulting from within-channel (Q_{chnl}) and floodplain (Q_{fldp}) inputs at the upstream end.

$$Q(t) = Q_{h,surf}(t) + Q_{h,base}(t) + Q_{chnl}(t) + Q_{fldp}(t) \qquad (15)$$

The above process is carried out sequentially, starting from the most upstream reaches and proceeding to the downstream reaches.

3.4. Overall Model Implementation

[29] Grid-based meteorological and land cover data were mapped to the catchment template using areal averaging relationships determined using a GIS. The catchment-based CLM was implemented over the study area and simulations were performed for the period 1949–1960 using 1 h time steps. All model parameters in the catchment-based CLM were the same as those in the default grid-based CLM. In

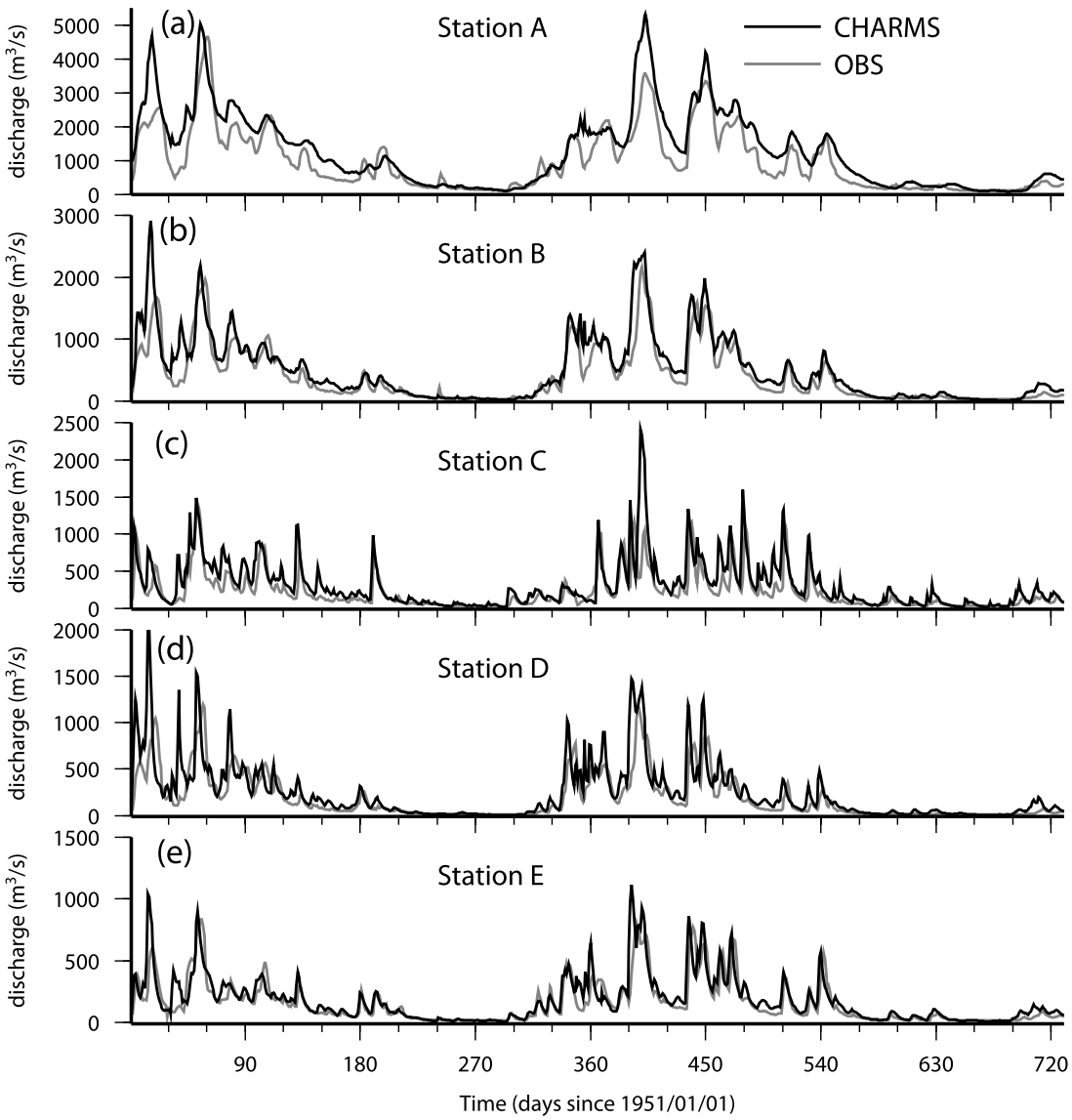

Figure 4. (a) Comparison of simulated daily streamflow (in $m^3\ s^{-1}$) from CHARMS (black line) with observed daily streamflow (grey line) at station A. For ease of visualization only the first 2 years of simulated daily streamflow from the period 1951–1960 is presented here. (b–e) Same as Figure 4a but for stations B, C, D and E, respectively. Note that the scale of the *y* axis is not the same for all the panels.

order to minimize computations, the routing model was implemented using 6 h time steps. At the end of every 6 h period, surface and subsurface runoff from the catchment-based CLM was averaged over the 6-h period and was fed to the routing model. On the basis of preliminary simulations, the value of convective velocity V_c, given by (8), was scaled by a factor of 4.0 resulting in a better simulation of observed discharge. The first 2 years of the model simulation were discarded as the model spin-up period. Since observed streamflow data consists only of daily streamflow observations, simulated 6-hourly streamflow was aggregated to daily time steps for comparison.

4. Results

4.1. Simulation of Streamflow

[30] Simulated daily streamflow from CHARMS was compared with observed streamflow at gaging stations A–E for the period 1951–1960 (see Figure 4). It is evident that daily streamflow from CHARMS captures the seasonal variability reasonably well. This is reflected in the performance statistics for daily streamflow (Table 2). At the most downstream station (station A), the correlation coefficient

Table 2. Statistics of Model Performance for Daily Streamflow Simulation at the Five Stations (A, B, C, D and E) Shown in Figure 1[a]

Station	*r*	*RMSE*	*ME*
A	0.92	468	0.65
B	0.90	224	0.64
C	0.77	207	0.25
D	0.76	190	0.10
E	0.82	108	0.56

[a] *r* is correlation coefficient, *RMSE* is root mean squared error (in $m^3\ s^{-1}$), and *ME* is modeling efficiency or the Nash-Sutcliffe coefficient.

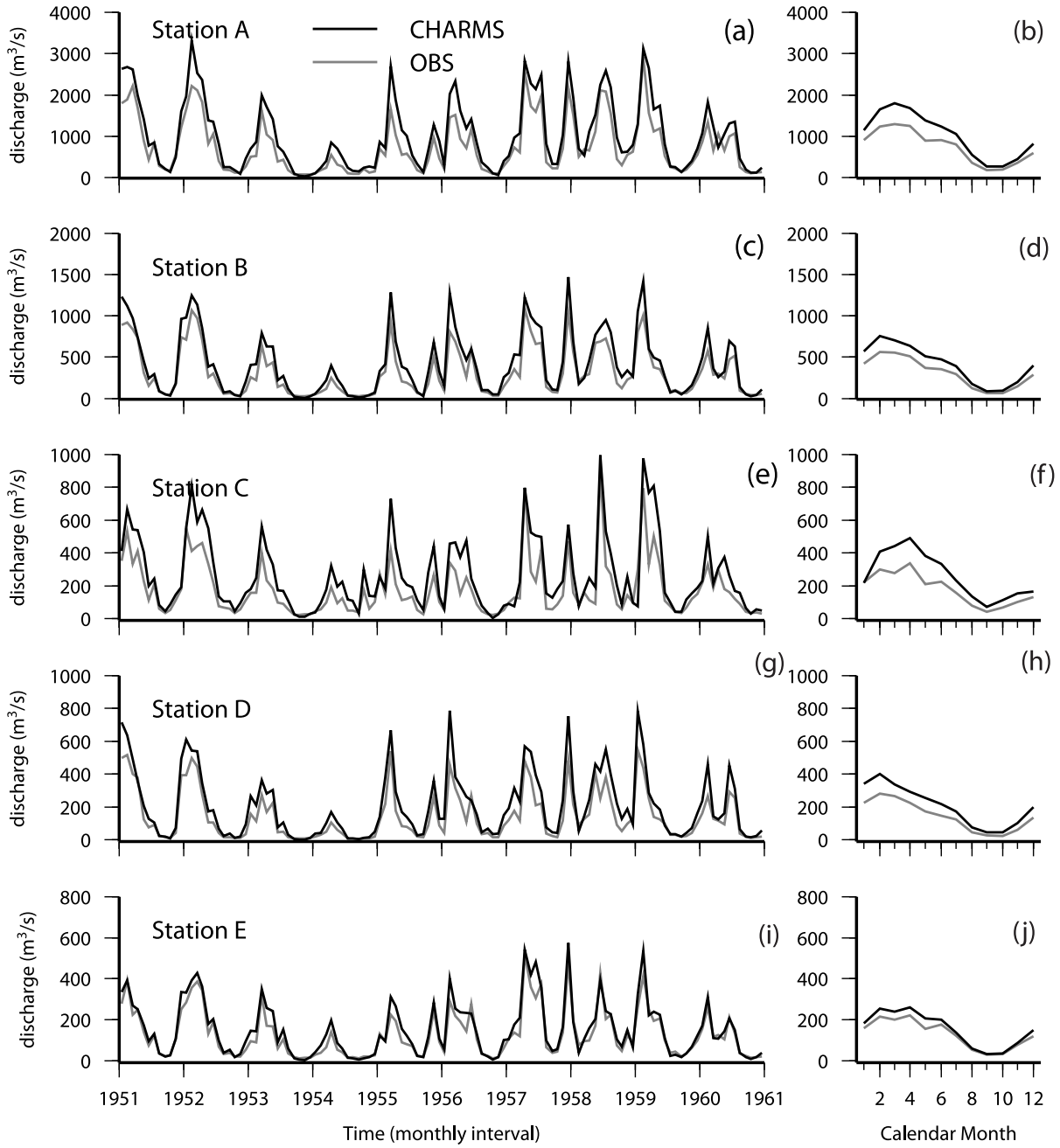

Figure 5. (a) A comparison of simulated monthly streamflow (in $m^3\ s^{-1}$) from CHARMS (black line) with observations (grey line) at station A. (b) Same data averaged over each calendar month for the period 1951–1960. (d–j) Same as Figures 5a and 5b but for stations B, C, D and E, respectively. Note that the scale of the *y* axis is not the same for all the panels.

(*r*) is 0.92, the root mean squared error (*RMSE*) is 444 $m^3\ s^{-1}$ and the Nash-Sutcliffe coefficient is 0.69 (see Table 2). Similar performance of CHARMS at other measurement stations (stations B through E) suggests that CHARMS can reproduce observed daily streamflow well, with correlation coefficients ranging from 0.76 at station D to 0.92 at station A. Because of the higher runoff generated by the CLM during the high-flow seasons (winter and spring), CHARMS typically overestimates runoff and misses some of the observed peaks in the daily streamflow.

[31] Simulated monthly streamflow from CHARMS, and the corresponding mean of the monthly streamflow averaged over the 10 year simulation period, are compared with observations in Figure 5. As expected, the performance statistics for monthly simulations are better than those for the daily simulations (Table 3). CHARMS can reproduce observed monthly streamflow with *r* ranging from 0.94 at station C to 0.98 at station B. Again, because of the higher runoff generated by the CLM during the winter and spring, CHARMS overestimates observed discharge in these seasons. The low season flow in the summer and fall (July

Table 3. Same as Table 2 Except That the Model Performance Statistics Are for Monthly Streamflow Simulations

Station	*r*	*RMSE*	*ME*
A	0.97	382	0.71
B	0.98	146	0.81
C	0.93	124	0.44
D	0.97	91	0.68
E	0.97	41	0.89

through December) is well captured by CHARMS at all the five HCDN stations. For the purposes of this study we consider the daily and monthly streamflow simulations from CHARMS to be representative of the observations.

[32] Other than changing the convective velocity, V_c, calibration of CLM runoff parameters [e.g., see *Niu et al.*, 2005] was not pursued because the main objective of this study is to demonstrate the general feasibility of CHARMS and its routing model in the context of climate simulation, where significant parameter tuning is unlikely. The effect of scaling V_c on the simulated streamflow at station A is demonstrated in Figure 6. It is evident from Figure 6 that scaling of V_c results in a gradual variation in daily streamflow and closer resemblance to the observations (see Figure 4). At the monthly and mean monthly timescale, the effects of scaling V_c on the streamflow simulations are minimal. The above scaling factor is limited only to this study, and it must be viewed as a calibration factor to compensate for the fact that channel geometry and roughness are poorly resolved by the SRTM data. Also, convective velocity is dependent on geomorphic parameters such as channel roughness, which has been shown to be dependent on scale [e.g., *Molnar and Julien*, 2000]. Thus, the use of a constant scaling factor and a constant value of Manning's roughness coefficient for catchments of different sizes can be justified only from a utilitarian point of view. Future implementations of CHARMS would strive for improving the representation of channel geometry from SRTM in order to reduce reliance on scaling factors and enable dynamic estimation of velocity. For the purposes of this study we consider the daily and monthly streamflow simulations from CHARMS to be representative of the observations.

4.2. Simulation of Flow Depth and Inundation Extent

[33] In order to demonstrate the capability of CHARMS to provide information on river flow depth and channel inundation extent, two particular calendar years during the simulation period are considered. The year 1954 and 1957 were years of historical drought and flooding in Indiana [*Paulson et al.*, 1991] (also Figure 5), which contains most of the Wabash River basin (see Figure 1b).

[34] Simulated average monthly flow depth for the drought year of 1954 and the flood year of 1957 are shown in Figure 7. Within each year, higher discharge during the winter and spring seasons results in higher flow depth. Seasonal variation in flow depth is typically 2–3 m and flow depth generally increases from the upstream river channels to the downstream river channels. Within a river channel, increase in flow depth from the upstream to the downstream reaches is also evident in Figure 7. As expected, flow depth is generally higher during the flood year of 1957 than during the drought year of 1954. The annual variation in flow depth in the most downstream reaches of the Wabash basin is from 0 to 2 m in 1954 and from 1 to 4 m in 1957.

[35] The extent of inundation or flow width associated with the flow depth is shown in Figure 8. Width of flow is typically the smallest during the low flows of the summer

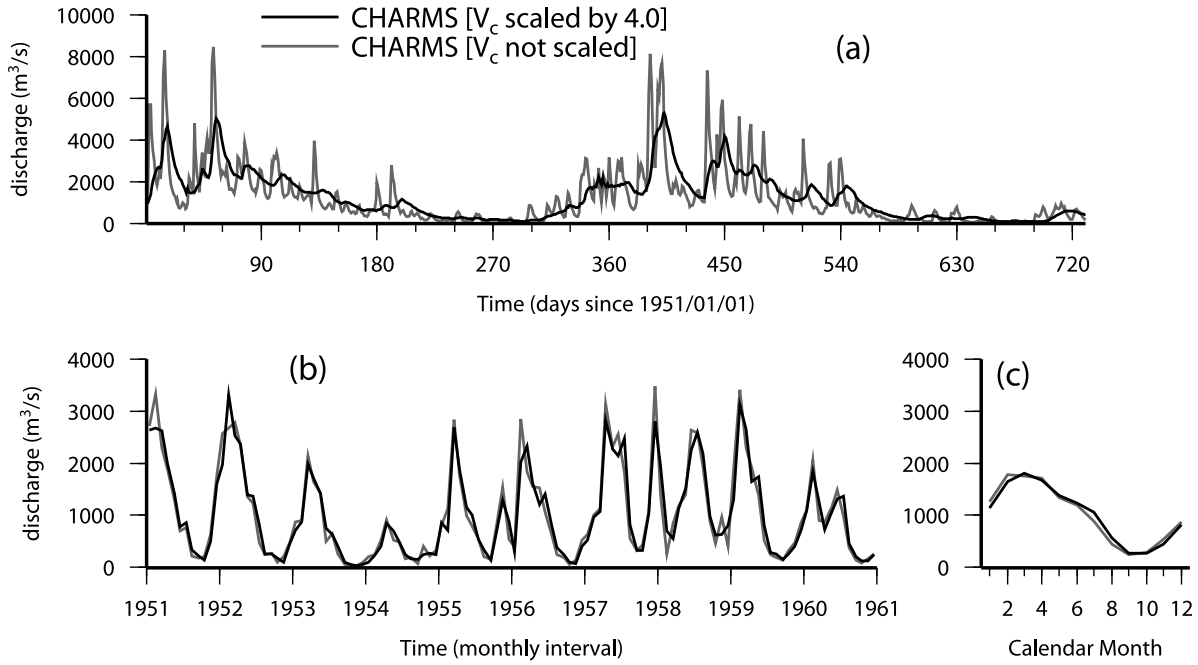

Figure 6. (a) Comparison of simulated daily streamflow (in $m^3\ s^{-1}$) from CHARMS with scaling V_c by a factor of 4.0 (black line) and without scaling V_c (grey line) at station A. (b) Same as Figure 6a but for monthly streamflow. (c) Same as Figure 6a but for mean monthly streamflow.

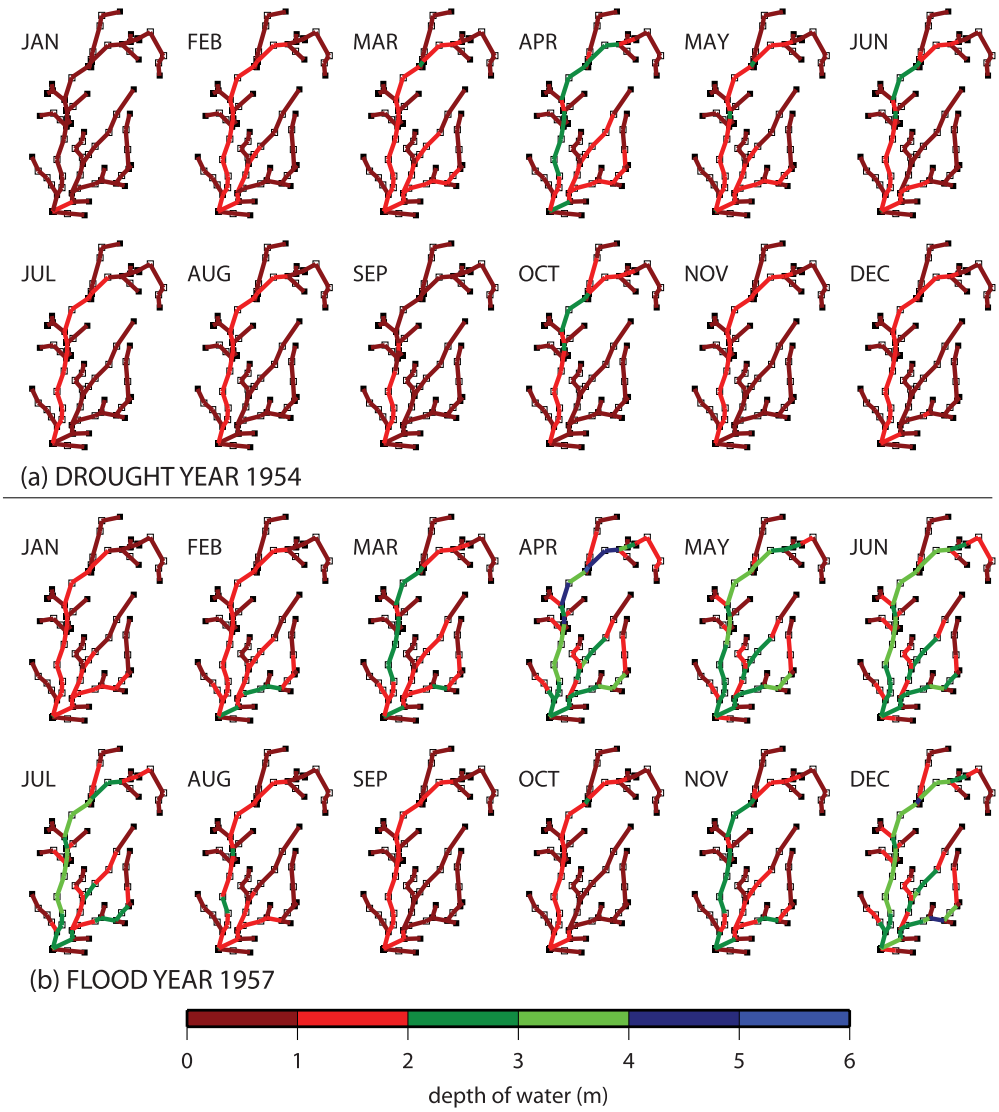

Figure 7. (a) Simulated average monthly flow depth for the drought year of 1954. (b) Same as Figure 7a but for the flood year of 1957.

season and highest during the peak flows of the spring season. As expected, inundation extent in the downstream reaches of the Wabash basin is greater during the flood year of 1957 than during the drought year of 1954. The annual variation in inundation extent in the most downstream reaches of the Wabash basin is from 100 to 700 m in 1954 and from 400 to 1600 m in 1957. Although higher discharge leads to higher flow depth, it does not always lead to a greater inundation width (e.g., in deeper, more straight-sided channels). Hence, seasonal variation in inundation extent need not be as dramatic as the seasonal variation in flow depth.

[36] In order to minimize the computations in the routing model, one effective cross-section profile was used per routing reach instead of using SRTM profiles available at every 1 km along the reach (see section 3.3.3). As shown in Figure 9, this could lead to an unrealistic estimation of flow depth and inundation extent. Corresponding to the simulated discharge at station A, flow depth and inundation extent obtained using the effective cross-section profile (for the routing reach in which station A is present) and the SRTM cross-section profile (at station A) are compared in Figure 9. The effective cross-section profile associated with station A is shallower and wider than the SRTM profile at station A.

[37] The simulated flow depth (see Figure 9b) and inundation extent (see Figure 9c), using the SRTM and effective profiles, follow the seasonal pattern of discharge, with lower (higher) values of depth and inundation extent during the drought (flood) year of 1954 (1957). Discharge exceeded the bankfull flow (see Figure 9a), for both the profiles, for a significant portion of the simulation period. This is also evident in the contribution of simulated floodplain discharge to the total discharge (see Figure 9d). These results suggest that additional improvements must be made to the channel cross-section characterization procedure and to the empirical flow partitioning approach (described in section 3.3.3). Nonetheless, the inclusion of the SRTM-

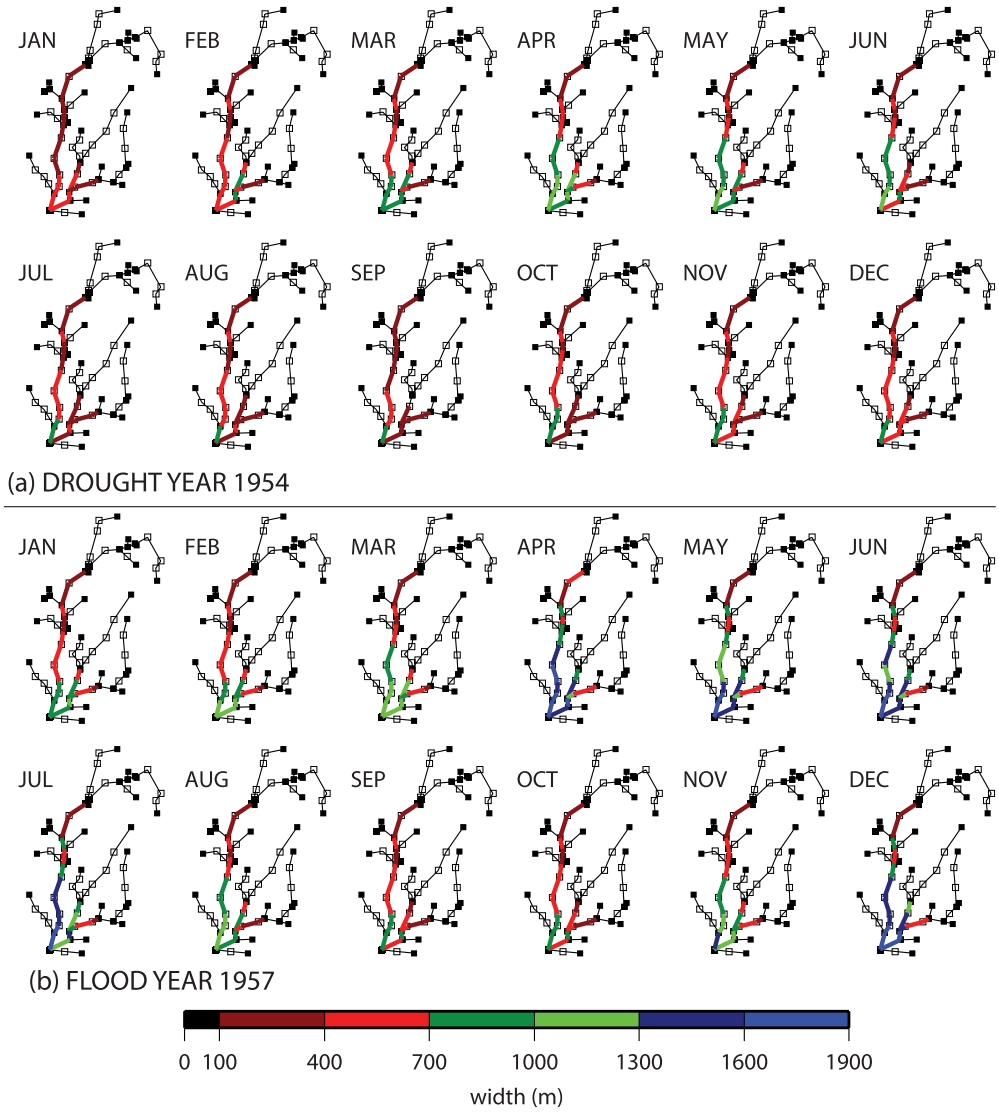

Figure 8. (a) Simulated average monthly inundation extent for the drought year of 1954. (b) Same as Figure 8a but for the flood year of 1957. Note that changes occur only within the river channels for which SRTM cross-section profiles were extracted (see Figure 3). The remainder of the channels have a width of 100 m with no provision for overbank flow.

derived channel geometry in CHARMS allowed for an initial estimation of flow depth, inundation extent and floodplain storage.

5. Discussion

[38] The routing model in CHARMS used several assumptions and scaling factors to account for the deficiencies in the cross-section profile data. For instance, the SRTM-derived channel width was adjusted by a factor of 0.5 and the width of the channels that could not be resolved using SRTM was assumed to be a constant value of 100 m (section 3.3.3). These adjustments were made for river reaches used in this study on the basis of comparisons with in situ cross-section data available at gauging stations. These assumptions are applicable only to this study and were made for the purpose of demonstrating the use of cross-section profile information in a continental-scale routing model. However, the need for adjustment of cross-section data indicates a major limitation of SRTM data in characterizing channel shape, particularly the bottom of the channel. A more generic adjustment method that ensures accurate representation of the channel shape with SRTM data is required prior to a global implementation of CHARMS. Such a method would require extensive validation with in situ cross-section data (e.g., from USGS in the United States, from ANEEL in Brazil, etc.), data from internet databases (e.g., Global Hydrographic Array, http://www.dartmouth.edu/floods/reaches/index.html), and empirical relationships from the literature [e.g., *Hey*, 1988; *Bjerklie et al.*, 2005].

6. Summary

[39] Toward the long-term objective of simulating spatio-temporal variations in global surface water storage and

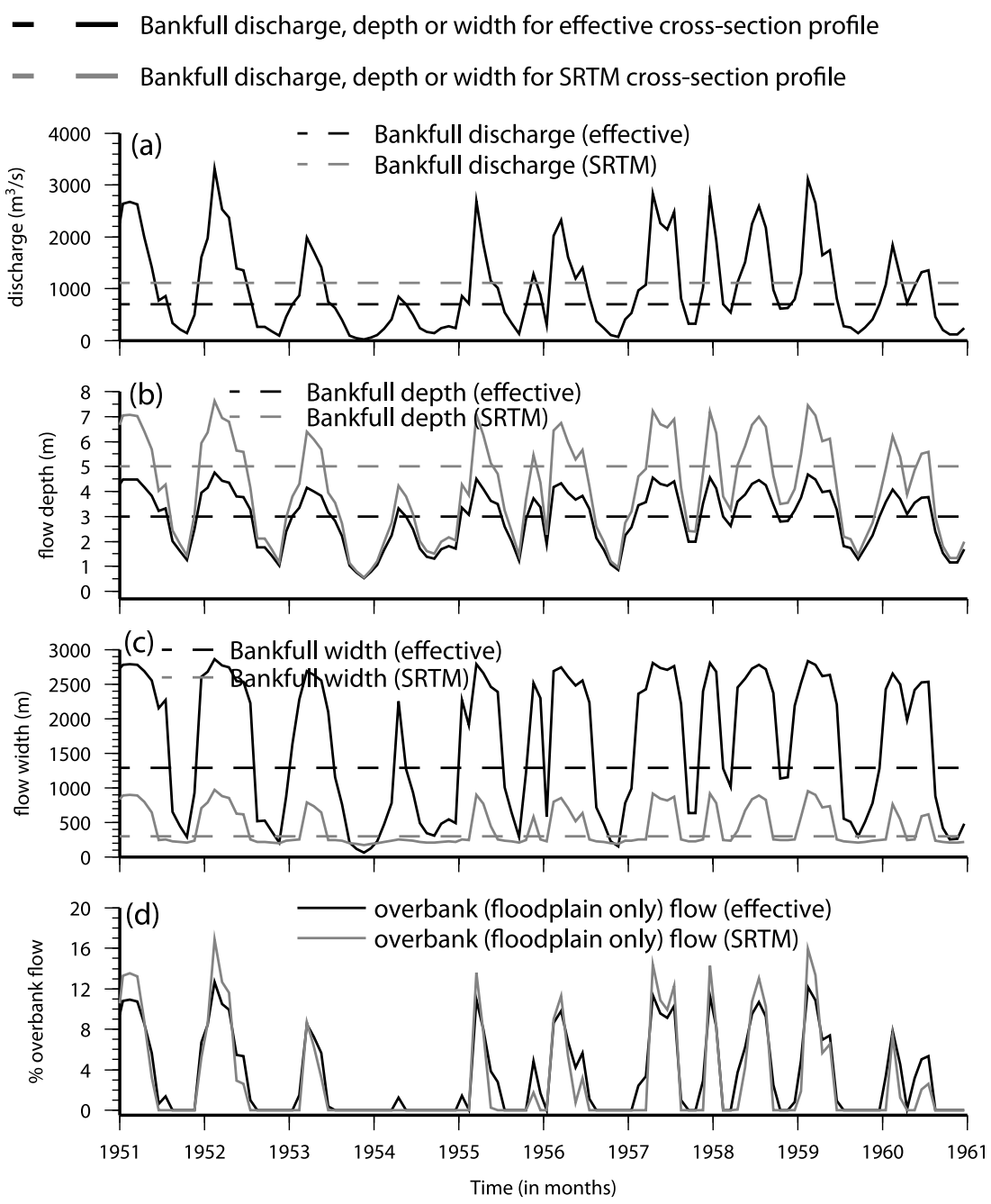

Figure 9. (a) Simulated monthly discharge at station A. The black broken line and the grey broken line indicate the bankfull discharge corresponding to the effective and SRTM cross-section profiles, respectively. (b) The black line and the grey line indicate monthly simulated flow depth corresponding to the effective and SRTM cross-section profiles, respectively, and the broken lines indicate the corresponding bankfull depth. (c) Same as Figure 9b but for monthly simulated inundation extent. (d) Simulated monthly overbank flow as a fraction of simulated total monthly discharge.

extent, we present a catchment-based land surface modeling framework with explicit representation of storage and movement of water in river channels and floodplains. The overall framework, called CHARMS, is composed of a land surface model and a river routing model that operate on a network of hydrologic catchments. The routing model in CHARMS has an accurate representation of river flow paths and has the ability to utilize channel cross-section geometry for the simulation of river discharge and associated flow depth and inundation extent. Effects of overland, subsurface, river channel and floodplain transport processes on the magnitude and timing of streamflow are considered by the routing model. The CHARMS framework will ultimately enable assimilation of satellite observations of surface water heights and inundation extents, the incorporation of water

management practices such as reservoir storage, linkages to biogeochemical processes and related feedbacks to climate.

[40] CHARMS was implemented over the Wabash River basin, and simulated streamflow was validated using daily observations. Using cross-section profile information extracted from the 90 m SRTM DEM, river flow depth and inundation extent associated with the simulated discharge were estimated and were found to be generally following observed flooding and droughts. This study is the first of its kind to utilize information on river flow paths and river channel cross-section geometry and explicitly simulate depth and inundation extent associated with discharge in river channels, all within a land surface model in a global climate modeling framework.

[41] **Acknowledgments.** The authors would like to thank the NASA Earth System Science Fellowship program and the computations supported by Earth System Modeling Facility NSF ATM-0321380.

References

Andreadis, K. M., E. A. Clark, D. P. Lettenmaier, and D. E. Alsdorf (2007), Prospects for river discharge and depth estimation through assimilation of swath-altimetry into a raster-based hydrodynamics model, *Geophys. Res. Lett.*, *34*, L10403, doi:10.1029/2007GL029721.

Asante, K. O. (2000), Approaches to continental scale river flow routing, Ph.D. dissertation, Univ. of Tex., Austin.

Asante, K. O., G. Artan, S. Pervez, C. Bandaragoda, and J. Verdin (2007), Technical manual of the Geospatial Streamflow Model (GeoSFM), *USGS Open File Rep.*, *OF 2007-1441*.

Bates, P. D., and A. P. J. DeRoo (2000), A simple raster-based model for flood inundation simulation, *J. Hydrol.*, *236*(1–2), 54–77.

Becker, A., and Z. W. Kundzewicz (1987), Nonlinear flood routing with multilinear models, *Water Resour. Res.*, *23*(6), 1043–1048.

Birkett, C. M., L. A. K. Mertes, T. Dunne, M. H. Costa, and M. J. Jasinski (2002), Surface water dynamics in the Amazon Basin: Application of satellite radar altimetry, *J. Geophys. Res.*, *107*(D20), 8059, doi:10.1029/2001JD000609.

Bjerklie, D. M., D. Moller, L. C. Smith, and S. L. Dingman (2005), Estimating discharge in rivers using remotely sensed hydraulic information, *J. Hydrol.*, *309*, 191–209.

Bonan, G. B., K. W. Oleson, M. Vertenstein, S. Levis, X. Zeng, Y. Dai, R. E. Dickinson, and Z. Yang (2002), The land surface climatology of the community land model coupled to the NCAR community climate model, *J. Clim.*, *15*, 3123–3149.

Chen, J., and P. Kumar (2001), Topographic influence on the seasonal and interannual variation of water and energy balance of basins in North America, *J. Clim.*, *14*, 1989–2014.

Chow, V. T. (Ed.) (1959), *Open-Channel Hydraulics*, McGraw-Hill, New York.

Coe, M. T., and G. Bonan (1997), Feedbacks between climate and surface water in northern Africa during the middle Holocene, *J. Geophys. Res.*, *102*, 11,087–11,101.

Coe, M. T., M. H. Costa, A. Botta, and C. Birkett (2002), Long-term simulations of discharge and floods in the Amazon Basin, *J. Geophys. Res.*, *107*(D20), 8044, doi:10.1029/2001JD000740.

Cunge, J. A., F. M. Holly, and A. Verwey (Eds.) (1980), *Practical Aspects of Computational River Hydraulics*, Iowa Inst. of Hydraul. Res., Iowa City, Iowa.

Doll, P., F. Kaspar, and B. Lehner (2003), A global hydrological model for deriving water availability indicators: Model tuning and validation, *J. Hydrol.*, *270*, 105–134.

Famiglietti, J. S., and E. F. Wood (1994), Multi-scale modeling of spatially variable water and energy balance processes, *Water Resour. Res.*, *30*(11), 3061–3078.

Farr, T. G., et al. (2007), The Shuttle Radar Topography Mission, *Rev. Geophys.*, *45*, RG2004, doi:10.1029/2005RG000183.

Fekete, B., C. J. Vorosmarty, and W. Grabs (2002), High resolution fields of global runoff combining observed river discharge and simulated water balances, *Global Biogeochem. Cycles*, *16*(3), 1042, doi:10.1029/1999GB001254.

Fread, D. L. (1993), Flow routing, in *Handbook of Hydrology*, 1st ed., edited by D. R. Maidment, pp. 10.1–10.36, McGraw-Hill, New York.

Garbrecht, J. (1990), Analytical representation of cross-section hydraulic properties, *J. Hydrol.*, *119*, 43–56.

Garbrecht, J., and G. Brunner (1991), Hydrologic channel-flow routing for compound sections, *J. Hydraul. Eng. ASCE*, *117*(5), 629–642.

Green, P. A., C. J. Vorosmarty, M. Meybeck, J. N. Galloway, B. J. Peterson, and E. W. Boyer (2004), Pre-industrial and contemporary fluxes of nitrogen through rivers: A global assessment based on typology, *Biogeochemistry*, *68*, 71–105.

Hanasaki, N., S. Kanae, and T. Oki (2006), A reservoir operation scheme for global river routing models, *J. Hydrol.*, *327*, 22–41.

Hey, R. D. (1988), Mathematical models of channel morphology, in *Modelling Geomorphological Systems*, 1st ed., edited by M. G. Anderson, pp. 99–125, John Wiley, Hoboken, N. J.

Jenson, S. K., and J. O. Domingue (1988), Extracting topographic structure from digital elevation data for geographic information system analysis, *Photogramm. Eng. Remote Sens.*, *54*(11), 1593–1600.

Keefer, T. N., and R. S. McQuivey (1974), Multiple linearization flow routing model, *J. Hydraul. Eng. ASCE*, *100*(7), 1031–1046.

Kite, G. W., A. Dalton, and K. Dion (1994), Simulation of streamflow in a macroscale watershed using general circulation model data, *Water Resour. Res.*, *30*(5), 1547–1559.

Koster, R. D., M. J. Suarez, A. Ducharne, M. Stieglitz, and P. Kumar (2000), A catchment-based approach to modeling land surface processes in a GCM: 1. Model structure, *J. Geophys. Res.*, *105*, 24,809–24,822.

Lee, K. T., and C. Chang (2005), Incorporating subsurface-flow mechanism into geomorphology-based IUH modeling, *J. Hydrol.*, *311*, 91–105.

Lehner, B., K. Verdin, and A. Jarvis (2006), Hydrosheds technical documentation, Wildlife Fund U.S., Washington, D. C. (Available at http://hydrosheds.cr.usgs.gov)

Lohmann, D., R. Nolte-Holube, and E. Raschke (1996), A large-scale horizontal routing model to be coupled to land surface parametrization schemes, *Tellus, Ser. A*, *48*, 708–721.

Maidment, D. R. (Ed.) (2002), *Arc Hydro: GIS for Water Resources*, 1st ed., ESRI Press, Redlands, Calif.

Maurer, E. P., A. W. Wood, J. C. Adam, D. P. Lettenmaier, and B. Nijssen (2002), A long-term hydrologically-based data set of land surface fluxes and states for the conterminous United States, *J. Clim.*, *15*, 3237–3251.

Miguez-Macho, G., Y. Fan, C. P. Weaver, R. Walko, and A. Robock (2007), Incorporating water table dynamics in climate modeling: 2. Formulation, validation, and soil moisture simulation, *J. Geophys. Res.*, *112*, D13108, doi:10.1029/2006JD008112.

Miller, J. R., G. L. Russell, and G. Caliri (1994), Continental-scale river flow in climate models, *J. Clim.*, *7*, 914–928.

Molnar, D. K., and P. Y. Julien (2000), Grid-size effects on surface runoff modeling, *J. Hydrol. Eng.*, *5*(1), 8–16.

Niu, G. Y., Z. L. Yang, R. E. Dickinson, and L. E. Gulden (2005), A simple topmodel-based runoff parameterization (SIMTOP) for use in global climate models, *J. Geophys. Res.*, *110*, D21106, doi:10.1029/2005JD006111.

Olivera, F., and D. Maidment (1999), Geographic information systems (GIS)-based spatially distributed model for runoff routing, *Water Resour. Res.*, *35*(4), 1155–1164.

Olivera, F., J. Famiglietti, and K. Asante (2000), Global-scale flow routing using a source-to-sink algorithm, *Water Resour. Res.*, *36*(8), 2197–2207.

Paulson, R. W., E. B. Chase, R. S. Roberts, and D. W. Moody (1991), National water summary 1988–89—Hydrologic events and floods and droughts, *U. S. Geol. Surv. Water Supply Pap. 2375*.

Prigent, C., F. Papa, F. Aires, W. B. Rossow, and E. Matthews (2007), Global inundation dynamics inferred from multiple satellite observations, 1993–2000, *J. Geophys. Res.*, *112*, D12107, doi:10.1029/2006JD007847.

Rahmstorf, S. (1996), On the freshwater forcing and transport of the Atlantic thermohaline circulation, *Clim. Dyn.*, *12*, 799–811.

Reichle, R. H., and R. D. Koster (2005), Global assimilation of satellite surface soil moisture retrievals into the NASA Catchment land surface model, *Geophys. Res. Lett.*, *32*, L02404, doi:10.1029/2004GL021700.

Richey, J. E., J. M. Melack, A. K. Aufdenkampe, V. M. Ballester, and L. L. Hess (2002), Outgassing from Amazonian rivers and wetlands as a large source of tropical CO_2, *Nature*, *416*, 617–620.

Sheffield, J., G. Goteti, and E. F. Wood (2006), Development of a 50-yr high-resolution global dataset of meteorological forcings for land surface modeling, *J. Clim.*, *19*(13), 3088–3111.

Slack, J. R., and J. M. Landwehr (1992), Hydro-Climatic Data Network: A U. S. Geological Survey streamflow data set for the United States for the study of climatic variations, 1874–1988, *U. S. Geol. Surv. Open File Rep.*, *92-129*.

Syvitski, J. P. M., C. J. Vorosmarty, A. J. Kettner, and P. Green (2005), Impact of humans on the flux of terrestrial sediment to the global coastal ocean, *Science*, *308*, 376–380.

Vorosmarty, C. J., B. Moore, A. L. Grace, M. P. Gildea, J. M. Melillo, B. J. Peterson, E. B. Rastetter, and P. A. Steudler (1989), Continental scale

model of water balance and fluvial transport: An application to South America, *Global Biogeochem. Cycles*, *3*(3), 241–265.
Yu, Z. B., D. Pollard, and L. Cheng (2006), On continental-scale hydrologic simulations with a coupled hydrologic model, *J. Hydrol.*, *331*(1–2), 110–124.

K. Asante, Geospatial Science and Engineering, South Dakota State University, Brookings, SD 57007, USA.

J. S. Famiglietti and G. Goteti, Department of Earth System Science, University of California, 1101 Croul Hall, Irvine, CA 92697, USA. (jfamigli@uci.edu)